

The Influence of Intrinsic Strain Softening on Strain Localization in Polycarbonate: Modeling and Experimental Validation

L. E. Govaert

Eindhoven University of Technology,
Faculty of Mechanical Engineering,
P.O. Box 512, 5600 MB Eindhoven,
The Netherlands

P. H. M. Timmermans

Philips Center for Manufacturing Technology,
Eindhoven, The Netherlands

W. A. M. Brekelmans

Eindhoven University of Technology,
Faculty of Mechanical Engineering,
P.O. Box 512, 5600 MB Eindhoven,
The Netherlands

Intrinsic strain softening appears to be the main cause for the occurrence of plastic localization phenomena in deformation of glassy polymers. This is supported by the homogeneous plastic deformation behavior that is observed in polycarbonate samples that have been mechanically pretreated to remove (saturate) the strain softening effect. In this study, some experimental results are presented and a numerical analysis is performed simulating the effect of mechanical conditioning by cyclic torsion on the subsequent deformation of polycarbonate. To facilitate the numerical analysis of the "mechanical rejuvenation" effect, a previously developed model, the "compressible Leonov model," is extended to describe the phenomenological aspects of the large strain mechanical behavior of glassy polymers. The model covers common observable features, like strain rate, temperature and pressure dependent yield, and the subsequent strain softening and strain-hardening phenomena. The model, as presented in this study, is purely "single mode" (i.e., only one relaxation time is involved), and therefore it is not possible to capture the nonlinear viscoelastic pre-yield behavior accurately. The attention is particularly focused on the large strain phenomena. From the simulations it becomes clear that the preconditioning treatment removes the intrinsic softening effect, which leads to a more stable mode of deformation. [S0094-4289(00)01002-1]

1 Introduction

The deformation behavior of glassy polymers is generally strongly dominated by localization phenomena like necking, shear band formation, or crazing. This susceptibility to localization is directly related to the intrinsic large strain behavior of glassy polymers visualized in Fig. 1. These true stress-strain curves can be obtained in uniaxial extension using a video-controlled tensile test [1] or in uniaxial compression [2,3]. Typically, the yield stress depends on strain rate, temperature, and pressure [4]. The post-yield behavior of glassy polymers is governed by two characteristic phenomena [1,5]. Immediately after the yield point the (true) stress tends to decrease with increasing deformation, an effect that is usually referred to as intrinsic strain softening. At large deformations the softening effect is saturated and the true stress starts to rise again with increasing deformation. This strain hardening effect has been subject of a number of studies in the past (e.g., [3,6,7]), and is generally interpreted as a rubber elastic contribution by the molecular entanglement network.

Although the origin of the intrinsic softening effect is not yet completely clear, it seems to be closely related to the physical aging process (volume relaxation) that occurs in the glassy state [8]. With physical aging the specific volume decreases leading to an increase of the elastic modulus, a decrease of the time dependence (age-shift), and an increase of the yield stress [8]. The increase of the yield stress seems to develop simultaneously with the enthalpy overshoot that is observed around the glass transition temperature in DSC experiments on aged amorphous polymers [9,10]. The effect of aging on the deformation behavior of a glassy polymer is schematically represented in Fig. 2. During aging, the yield stress increases and the intrinsic softening effect appears. As a result of intrinsic softening the large strain behavior

of the different samples is exactly the same: the effect of physical aging has been removed and the material is rejuvenated [10–12]. The same effect can be achieved by heating the sample above the glass transition temperature and cooling it rapidly to the glassy state (quenching). In some glassy polymers, as, for instance, PVC, intrinsic softening completely disappears after this quenching from the rubbery into the glassy state [13].

Although these experimental observations clearly connect the intrinsic softening effect to the physical aging process, the effect cannot be rationalized completely in terms of an increase of free volume as a result of the imposed strain. The inability to explain intrinsic softening in experiments with a negative dilatational strain (compression) is probably the strongest argument. Xie et al. [14] measured a decrease of the actual free volume in polycarbonate under compression by means of positron annihilation lifetime spectroscopy (PALS), whereas polycarbonate is known to display intrinsic softening in compression [3]. In PALS measurements during compression tests on polymethylmethacrylate, however, Hasan et al. [15] observed an increase of the number of areas of local free volume evolving to a steady value. Based upon these observations they postulated a phenomenological law for the evolution of the density D of these areas in a glassy polymer during deformation. During elastic deformation, D is constant (the material state does not change). During plastic deformation, D evolves to a saturation value D_∞ , indicating a maximum amount of regions with elevated levels of free volume, which is independent of strain rate or thermal history. Inclusion of D in an originally non-intrinsic softening model resulted in a constitutive model that exhibited intrinsic strain softening [15].

Intrinsic strain softening is an important factor in the initiation of strain localization. As during softening the deformation is allowed to proceed at a decreasing level of the (true) stress, small stress variations will inherently lead to large differences in the local strain rate, nuclei for localized plastic deformation zones. In the absence of intrinsic softening, the deformation will be homogeneous if the strain-hardening behavior is large enough to com-

Contributed by the Materials Division for publication in the JOURNAL OF ENGINEERING MATERIALS AND TECHNOLOGY. Manuscript received by the Materials Division May 5, 1999; revised manuscript received November 23, 1999. Associate Technical Editor: H. M. Zbib.

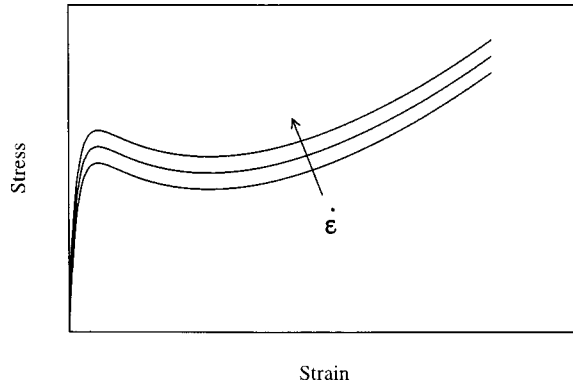


Fig. 1 Schematic representation of the effect of strain rate on the true stress-strain curve of a glassy polymer

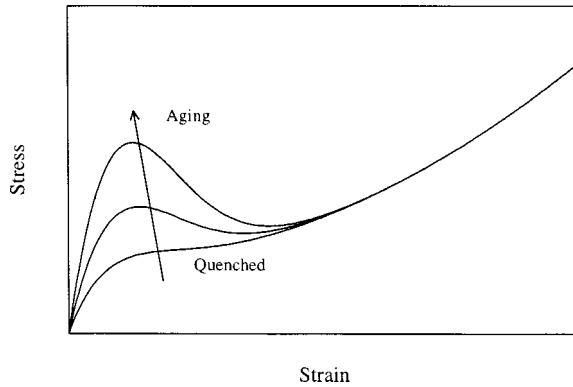


Fig. 2 Schematic representation of the effect of physical aging on the true stress-strain curve of a glassy polymer

pensate for the geometrical softening during a tensile test [4,7]. An extensive numerical study on the influence of strain softening and strain hardening on neck formation in plane strain extension was performed by Wu and van der Giessen [16]. They showed that intrinsic strain softening always leads to strain localization, whereas in the absence of softening strain localization can be suppressed if the amount of strain hardening is sufficient.

There is also some experimental evidence concerning the influence of strain softening on neck formation. Cross and Haward [13] used samples of quenched PVC that display no intrinsic softening and observed uniform deformation in a tensile test whereas slowly cooled samples necked. An alternative method to prevent inhomogeneous behavior in glassy polymers is based on the initial elimination of intrinsic softening by raising the value of the softening parameter D to its saturation value D_∞ by application of plastic deformation (mechanical preconditioning). A good example of the effect of mechanical preconditioning is the alternated bending of PVC samples by Bauwens [17], which suppressed necking in a subsequent tensile test. G'Sell [11] achieved the same effect after plastic cycling in simple shear on polycarbonate. Recent experimental research [18] also shows the effect of the elimination of intrinsic softening by mechanical preconditioning: axisymmetrical samples were plastically cycled in torsion; tensile tests on these rejuvenated samples resulted in homogeneous deformations and allowed for the characterization of the strain hardening behavior of polycarbonate.

The present study addresses the influence of intrinsic strain softening on the macroscopic deformation behavior of axisymmetric polycarbonate bars. To facilitate a numerical analysis, a constitutive model which was derived in a previous study, the so-called compressible Leonov model [19], is extended to incor-

porate the phenomena of intrinsic strain softening and strain hardening. The material characterization, including the determination of the necessary parameters for the extended model, will be discussed. With the parameters for polycarbonate known, the model is employed to simulate neck formation and to predict the deformation behavior of a mechanically preconditioned sample (torsion cycling) in a subsequent tensile or torsion test.

2 Constitutive Modeling

2.1 The Compressible Leonov Model. For an arbitrary material element of a loaded configuration the local actual deformation with respect to a predefined reference state is determined by the deformation gradient tensor \mathbf{F} (e.g., Hunter [20]). This tensor \mathbf{F} is multiplicatively decomposed into an elastic part \mathbf{F}_e and a plastic part \mathbf{F}_p , according to:

$$\mathbf{F} = \mathbf{F}_e \cdot \mathbf{F}_p \quad (1)$$

The plastic contribution \mathbf{F}_p indicates the deformation (with respect to the reference state) of the relaxed stress-free configuration, which is defined as the state that would instantaneously be recovered when the stress is suddenly removed from the element considered. The decomposition in Eq. (1) is not unique because rotational effects can be assigned to \mathbf{F}_p as well as to \mathbf{F}_e . Uniqueness is achieved by the extra requirement that the plastic deformation occurs spin-free [21].

The Cauchy stress tensor $\boldsymbol{\sigma}$ is elastically expressed in the left Cauchy Green tensor \mathbf{B}_e associated with the tensor \mathbf{F}_e which is defined by

$$\mathbf{B}_e = \mathbf{F}_e \cdot \mathbf{F}_e^c \quad (2)$$

where \mathbf{F}_e^c denotes the conjugate of \mathbf{F}_e (which is equivalent to the transpose of the matrix representation of the tensor). In this equation it is presupposed that the elastic behavior is isotropic. In that case the application of expressions of the type $\boldsymbol{\sigma} = \boldsymbol{\sigma}(\mathbf{B}_e)$ guarantees the conservation of objectivity (if indeed the total spin and consequently superimposed rigid body rotations are completely attributed to the elastic part of the deformation).

To specify the dependence of the stress on the deformation, a neo-Hookean relationship is chosen [19]:

$$\boldsymbol{\sigma} = K(J_e - 1)\mathbf{I} + G\tilde{\mathbf{B}}_e^d \quad (3)$$

where the superscript d indicates the deviatoric part.

In this equation, K and G are the bulk modulus and the shear modulus, respectively. The elastic volume change factor J_e is defined by

$$J_e = \det(\mathbf{F}_e) = \sqrt{\det(\mathbf{B}_e)} \quad (4)$$

The tensor $\tilde{\mathbf{B}}_e$ denotes the isochoric fraction of the elastic left Cauchy Green tensor \mathbf{B}_e according to

$$\tilde{\mathbf{B}}_e = J_e^{-2/3} \mathbf{B}_e \quad (5)$$

Based on purely kinematical considerations [19] the following differential equation can be derived to calculate the evolution of $\tilde{\mathbf{B}}_e$:

$$\dot{\tilde{\mathbf{B}}}_e = (\mathbf{D}^d - \mathbf{D}_p^d) \cdot \tilde{\mathbf{B}}_e + \tilde{\mathbf{B}}_e \cdot (\mathbf{D}^d - \mathbf{D}_p^d) \quad (6)$$

The left-hand side of this equation represents the (objective) Jaumann derivative of the isochoric elastic left Cauchy Green tensor. The tensor \mathbf{D}_p denotes the plastic deformation rate tensor. The initial condition necessary for the solution of the differential equation (6) reads: $\tilde{\mathbf{B}}_e = \mathbf{I}$.

To complete the constitutive description the plastic deformation rate is expressed in the Cauchy stress by a generalized non-Newtonian flow rule [22]

$$\mathbf{D}_p = \frac{\boldsymbol{\sigma}^d}{2\eta(\tau_{eq})} \quad \text{with} \quad \tau_{eq} = \sqrt{\frac{1}{2} \text{tr}(\boldsymbol{\sigma}^d \cdot \boldsymbol{\sigma}^d)} \quad (7)$$

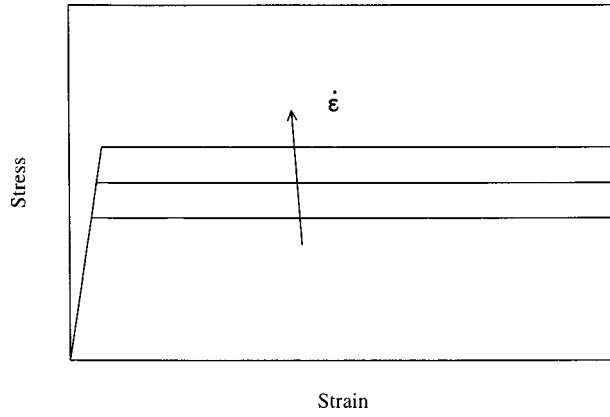


Fig. 3 Schematic representation of the response in uniaxial extension from the Leonov model

The viscosity η depends on the equivalent stress τ_{eq} according to an Eyring relationship [19]:

$$\eta(\tau_{eq}) = A \tau_0 \frac{\tau_{eq}/\tau_0}{\sinh(\tau_{eq}/\tau_0)} \quad (8)$$

In this equation A is a time constant and τ_0 a characteristic stress, respectively related to the activation energy ΔH and the shear activation volume V according to [4,20]

$$A = A_0 \exp\left[\frac{\Delta H}{RT}\right]; \quad \tau_0 = \frac{RT}{V} \quad (9)$$

with R the gas constant, A_0 a constant preexponential factor involving the fundamental vibration energy, and T the absolute temperature. It is emphasized that Eq. (7) implies that plastic deformation occurs at constant volume: $\text{tr}(\mathbf{D}_p) = 0$ as $\text{tr}(\boldsymbol{\sigma}^d) = 0$. Consequently \mathbf{D}_p^d in Eq. (6) may be replaced by \mathbf{D}_p . For the same reason, $J_e = \det(\mathbf{F}_e)$ in Eq. (3) may be replaced by $J = \det(\mathbf{F})$.

The model derived above was referred to as the compressible Leonov model in the original paper by Tervoort et al. [19]. To demonstrate the typical behavior of this compressible Leonov model, an application to uniaxial extension is performed. This leads, for constant strain rate, to the response schematically visualized in Fig. 3. The response of this Leonov model shows a sudden transition from elastic-to-plastic behavior, which is very similar to that of an elastic-perfectly plastic material with a rate-dependent yield stress.

2.2 Extension to Intrinsic Strain Softening and Strain Hardening. This section describes the extension of the compressible Leonov model to include both the intrinsic strain softening and the strain hardening effect. Complementary to the outline in Section 2.1 the Cauchy stress tensor $\boldsymbol{\sigma}$ is now redefined to be composed of two distinguishable parts (in a parallel assemblage), the driving stress tensor \mathbf{s} and the hardening stress tensor \mathbf{r} , according to

$$\boldsymbol{\sigma} = \mathbf{s} + \mathbf{r} \quad (10)$$

The expression for the driving stress \mathbf{s} is adopted from the compressible Leonov model described above, see Eq. (3):

$$\mathbf{s} = K(J-1)\mathbf{I} + G\tilde{\mathbf{B}}_e^d \quad (11)$$

The expression for the hardening stress \mathbf{r} is obtained in the following. In studies on the deformation behavior of glassy polymers, it is common practice to model the hardening behavior as a generalized rubber elastic spring with finite extensibility, like the so-called three-chain and eight-chain models of Arruda and Boyce [3], or the full chain model of Wu and van der Giessen [6]. On the other hand, Haward [7] applied network models employing

Gaussian chain statistics (leading to a neo-Hookean strain hardening response) to experimental uniaxial stress-strain curves, and concluded that some amorphous and most semicrystalline polymers obeyed this formulation. The large amount of softening, observed in some glassy polymers, prevented the successful application of the Gaussian model to these polymers. However, as mentioned in the Introduction, it can be shown by means of mechanical preconditioning [18] that this approach is also valid for polycarbonate. Gaussian statistics leads to a neo-Hookean relation between stresses and strains. Generalization to three dimensions, in the assumption that the network is incompressible, this neo-Hookean relationship for the hardening stress tensor \mathbf{r} can be written as

$$\mathbf{r} = H\tilde{\mathbf{B}}^d \quad (12)$$

with H the strain hardening modulus (assumed to be temperature independent). Contrary to Boyce et al. [21] the hardening stress is not related to the plastic deformation but to the total deformation. This adaptation is introduced because in the present approach both elastic and plastic deformations are assumed to decrease the configurational entropy of the polymer.

To complete the constitutive description the plastic deformation rate is still expressed in the Cauchy stress tensor by a generalized non-Newtonian flow rule

$$\mathbf{D}_p = \frac{\mathbf{s}^d}{2\eta(\tau_{eq}, D, p)} \quad (13)$$

where τ_{eq} , D , and p are state variables to be defined in the following.

Particularly the driving stress tensor \mathbf{s} is relevant for the incorporation of softening in the model. As suggested by Hasan et al. [15] a history variable D is specified, the softening parameter, which influences the viscosity η . During plastic deformation D evolves to a saturation level D_∞ , which is independent of the strain history. The result for η reads

$$\eta(\tau_{eq}, D, p) = A_m(D, p) \tau_0 \frac{\tau_{eq}/\tau_0}{\sinh(\tau_{eq}/\tau_0)} \quad (14)$$

where the equivalent stress τ_{eq} is redefined by

$$\tau_{eq} = \sqrt{\frac{1}{2} \text{tr}(\mathbf{s}^d \cdot \mathbf{s}^d)} \quad (15)$$

and with

$$A_m(D, p) = A \exp\left(\frac{\mu p}{\tau_0} - D\right) \quad (16)$$

$$p = -\frac{1}{3} \text{tr}(\boldsymbol{\sigma}) = -\frac{1}{3} \text{tr}(\mathbf{s}) \quad (17)$$

where p is the pressure (positive in compression). The parameter μ is a pressure coefficient, related to the shear activation volume V and the pressure activation volume Ω according to

$$\mu = \frac{\Omega}{V} \quad (18)$$

The evolution of the softening parameter D is specified by [15]

$$\dot{D} = h \left[1 - \frac{D}{D_\infty} \right] \dot{\gamma}_p \quad (19)$$

with initially $D=0$; h is a material constant describing the relative softening rate and $\dot{\gamma}_p$ is the equivalent plastic strain rate, according to

$$\dot{\gamma}_p = \sqrt{\text{tr}(\mathbf{D}_p \cdot \mathbf{D}_p)} = \frac{\tau_{eq}}{\eta\sqrt{2}} \quad (20)$$

3 Experimental

3.1 Materials and Sample Preparation. The material used in this study was polycarbonate, purchased as extruded rods (10.4 mm in diameter) from Eriks BV (Alkmaar, The Netherlands). Additional to the mechanical parameters K and G , the values of the density ρ , the thermal conductivity k , the thermal expansion coefficient α , the specific heat c , and the glass-transition temperature T_g are given in Table 1.

The material properties, with the exception of T_g , G , and K , were provided by the supplier and are in good agreement with values reported in literature [23–26]. T_g was determined by dynamic mechanical thermal analysis (DMTA) and G and K were determined from the Young's modulus E and the Poisson's ratio ν measured in the initial stages of a tensile test [19]. The thermal material parameters will be used to perform a thermomechanical analysis in the subsequent sections.

For the uniaxial extension and torsion experiments, the specimens were designed as dog-bone shaped axisymmetric bars, depicted in Fig. 4(a). For the uniaxial compression experiments, cylindrical test specimens were used, the geometry shown in Fig. 4(b).

3.2 Uniaxial Extension. Uniaxial tensile tests were performed on a FRANK 81656 tensile tester at strain rates varying from 10^{-4} to 10^{-2} [s^{-1}] and at temperatures of 22, 32, and 40 [$^{\circ}C$] (295, 305, and 313 [K], respectively). The true stress at the yield point, required for the determination of the yield parameters, was determined by assuming incompressibility in the viscoelastic area, which introduces a small error (approx. 2 percent) compared to a compressible approach. Neck formation and propagation was recorded by means of a video camera. From the images, the elongation factor in the neck is calculated from the diameter reduction in combination with the assumption of incompressibility. At the end of the test, the neck diameter was measured with the specimen still in the load frame as an assessment of the video images.

3.3 Uniaxial Compression. Uniaxial compression tests were performed at room temperature at strain rates in the range from 10^{-4} to 10^{-2} [s^{-1}], also on a FRANK 81656 tensile tester. A high performance lubricant (Hasco Z260) between the sample and the polished stainless-steel shaft of the compression device could not prevent the samples from barreling at compressive strains of approximately 0.20 [-]. Since this phenomenon occurred at compressive strains beyond the yield point, it does not affect the measured value of the true stress at the yield point. To avoid influence on the determination of the softening and hardening parameters, data measured at compressive strains beyond 0.20 [-] are omitted.

Table 1 Material properties of polycarbonate at room temperature

ρ [kg m ⁻³]	k [W m ⁻¹ K ⁻¹]	α [K ⁻¹]	c [J kg ⁻¹ K ⁻¹]	G [MPa]	K [MPa]	T_g [$^{\circ}C$]
1200	0.21	$65 \cdot 10^{-6}$	1200	860	4000	150

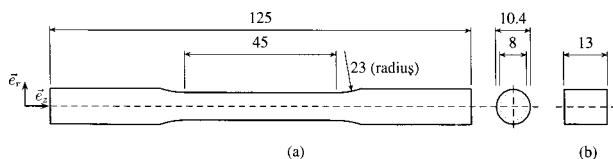


Fig. 4 Geometry of axisymmetrical specimens for (a) uniaxial extension and torsion experiments and (b) uniaxial compression experiments. Dimensions in [mm].

3.4 Torsion. Torsion experiments were performed on a testing machine consisting of an adjustable rigid support and a rotating clamp. The sample is installed in the machine in a way that initial axial forces in the sample are avoided. In the testing device the length of the sample is fixed during deformation and torque and axial load on the sample are measured during deformation by two independent load cells in the support. To determine the rotation, the angular displacement of the clamp is monitored. As a reference, an axial line was drawn on the specimen, and it appeared that the torsion was restricted to the gauge section of the sample. During the torsion of polycarbonate initially narrow circumferential shear bands were observed that broadened with ongoing rotation, a phenomenon that has also been reported by Wu and Turner [27]. In order to obtain isothermal conditions, the rotation speed was limited to 360 degrees per minute resulting in a nominal shear rate of 0.56 [s^{-1}] at the outer surface of the bar.

In the case of the mechanical pretreatment (rejuvenation), the torsion experiments were performed by twisting polycarbonate specimens to and fro over 720 degrees. After reversing the direction of the twist, the rotation rate was the same as during loading. Heating of the rejuvenated samples above the glass transition temperature did not induce any residual motion, from which it was concluded that the specimens rejuvenated in this way regain isotropy. After mechanical conditioning, the rejuvenated samples were allowed to relax unconstrained for 3 hrs. Subsequently, they were subjected to either uniaxial extension or torsion.

4 Material Characterization

4.1 Yield Parameters. The yield (or Eyring) parameters can be determined by measuring the true stress at the yield point during tension and compression experiments as a function of strain rate at different temperatures [28,29]. The strategy is based on the application of the incompressible non-Newtonian viscous flow rule, Eq. (13), which can be reformulated in axial direction (Fig. 4(a)) by

$$\frac{\dot{\lambda}_{p,zz}}{\lambda_{p,zz}} = \frac{1}{3\eta} (s_{zz} - s_{rr}) \quad (21)$$

with $\lambda_{p,zz}$ the axial plastic elongation factor and with s_{zz} and s_{rr} the axial and radial components of the driving stress tensor \mathbf{s} , respectively. The expression for the viscosity, Eq. (14), can then be replaced by:

$$\eta = \eta(s_{zz}, s_{rr}, p, D, T) = \frac{A \tau_0}{\exp\left[\frac{-\mu p}{\tau_0} + D\right]} \frac{\left[\frac{|s_{zz} - s_{rr}|}{\tau_0 \sqrt{3}}\right]}{\sinh\left[\frac{|s_{zz} - s_{rr}|}{\tau_0 \sqrt{3}}\right]} \quad (22)$$

To facilitate a straightforward analysis of the yield data, the following considerations are made:

- At the yield point, the contribution of hardening is negligible, and therefore the components of the driving stress are equal to the components of the Cauchy stress.
- At the yield point, the plastic strain rate is equal to the nominal strain rate $\dot{\epsilon}_{zz}^0$ applied.
- At the yield point the value of the softening parameter D equals 0.
- The argument of the hyperbolic sine in the viscosity function is large, and therefore the hyperbolic sine may be approximated by an exponential function.
- During uniaxial tension and compression, the pressure is given by $p = -1/3 \sigma_{zz}$.

The incorporation of these considerations into the non-Newtonian flow rule leads to

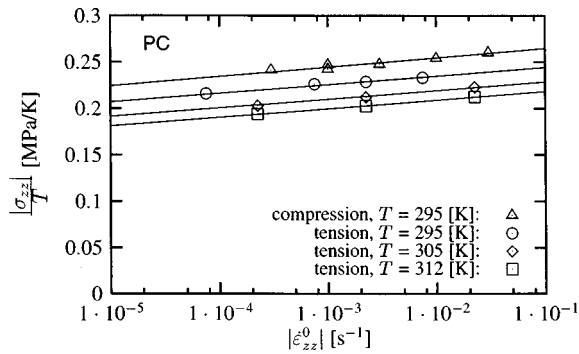


Fig. 5 Yield stress over absolute temperature $|\sigma_{zz}|/T$ as a function of strain rate $\dot{\epsilon}_{zz}$. The solid lines are a best fit using a single set of yielding parameters for each polymer.

Table 2 Yield parameters for polycarbonate

A_0 [s]	V [m ³ mol ⁻¹]	Ω [m ³ mol ⁻¹]	ΔH [kJ mol ⁻¹]
$3.6 \cdot 10^{-25}$	$3.4 \cdot 10^{-3}$	$2.4 \cdot 10^{-4}$	290

$$\frac{|\sigma_{zz}|}{T} = \frac{3R}{\sqrt{3}V + a\Omega} \left(\ln[A_0|\dot{\epsilon}_{zz}^0|] + \frac{\Delta H}{RT} - \ln\left[\frac{1}{6}\sqrt{3}\right] \right) \quad (23)$$

with $a = \text{sign}(\sigma_{zz})$. This expression suggests that plots of $|\sigma_{zz}|/T$ against the logarithm of the strain rate for a series of temperatures should give a set of parallel lines. The result for polycarbonate is shown in Fig. 5, where the measured values of $|\sigma_{zz}|/T$ of both the uniaxial tension as the uniaxial compression tests are plotted against the logarithm of $|\dot{\epsilon}_{zz}^0|$. The solid lines represent the best fit of the experimental results using a single set of the yield parameters A_0 , V , Ω , and ΔH , and seem to represent the actual yield behavior well over the entire range of strain rates experimentally covered. It should be noted however, that the yield parameters should be used with care outside the experimentally covered region, as it has been shown in experiments by Bauwens-Crowet et al. [29] that the yield stress of polycarbonate tends to have a more substantial strain rate and temperature dependence at low temperatures and high strain rates than observed at high temperatures and low strain rates. This is related to secondary glass-transitions and implies that actually more than one Eyring flow process should be taken into account. For the range of strain rates considered in the present work a single flow process seems to suffice.

The values of the yield parameters obtained from the fit are given in Table 2. The values are in good agreement with values reported by Bauwens-Crowet et al. [29] and Duckett et al. [28]

4.2 Hardening Parameter. As mentioned before in the Introduction, the hardening parameter H is, in the present study, determined from a uniaxial tensile test on a rejuvenated polycarbonate sample. To rejuvenate the material, axisymmetric samples were subjected to a 720 deg to and fro fixed-end torsion treatment. After this mechanical pretreatment the intrinsic strain softening behavior has disappeared (saturated) with the astonishing result that the polycarbonate bars deform homogeneously (without necking) in a subsequent tensile test. Figure 6 shows the result of such an experiment, where σ_{zz} is plotted as a function of the strain measure $\lambda_{zz}^2 - \lambda_{zz}^{-1}$. This strain measure is, in a uniaxial tensile (or compression) test, the component of the deviatoric isochoric left Cauchy Green deformation tensor $\tilde{\mathbf{B}}^d$ in the load direction \vec{e}_z . The constant slope of the tensile curve at large strain levels conse-

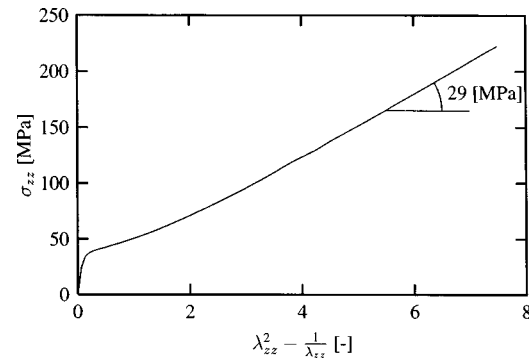


Fig. 6 True stress σ_{zz} versus $\lambda_{zz}^2 - \lambda_{zz}^{-1}$ during a tensile test at $\dot{\epsilon} = 2.2 \cdot 10^{-3}$ [s⁻¹] of a polycarbonate tensile bar, preconditioned in torsion

quently supports the neo-Hookean approach and directly reflects the value of the hardening modulus: $H = 29$ [MPa].

4.3 Strain Softening Parameters. The softening parameters of polycarbonate are provisionally determined from a uniaxial compression experiment. As was mentioned before, the uniaxial compression experiments showed barreling of the specimen at compressive strains over 0.2 [-] and therefore the data at larger compressive strains were omitted. The values of the softening parameters were determined by a fitting procedure on the post yield behavior of a compression test at a rate of 10^{-3} [s⁻¹]: $h = 200$ [-] and $D_\infty = 28$ [-] (see Fig. 7(a)). To facilitate the comparison with the experimental data, the predictions by the Leonov model were shifted along the strain axis in order to overlap the predicted and the measured yield points. The actual comparison between the experimental data and the prediction using the compressible Leonov model is shown in Fig. 7(b). The simulation was performed using the yield and hardening parameters obtained in the previous sections and the softening parameters mentioned above. Note the difference between the strains at yield in Fig. 7(b). Since the single mode compressible Leonov model displays elastic (rate independent) behavior up to the yield point, it is not able to describe the (multirelaxation time) viscoelastic behavior displayed by the material.

There are several possibilities to correct for this deficiency. One is the extension of the Leonov model to a spectrum of relaxation times (multimode) as was suggested by Tervoort et al. [30]. Another possibility was demonstrated by Hasan and Boyce [31] who considered a distribution of activation energies. As the use of either of these extensions would dramatically increase the computation time for the finite element analysis in the next sections the deficiency at low strain levels will not be addressed.

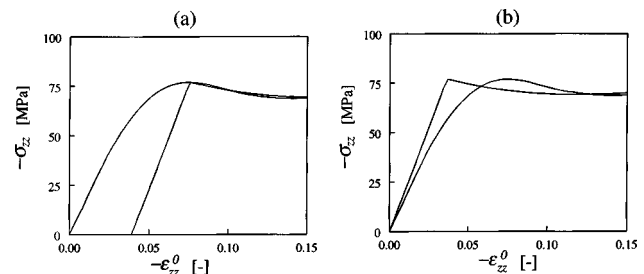


Fig. 7 Determination of the softening parameters in polycarbonate at a compressive strain rate of 10^{-3} [s⁻¹] at room temperature. (a) fitting the post-yield softening behavior; (b) simulation using the compressible Leonov model.

5 Numerical Simulations

5.1 Uniaxial Extension of Untreated Polycarbonate. For the analysis an axisymmetric specimen, as used in the experiments (Fig. 4), is considered. In the center of the bar, a Cartesian coordinate system is defined, in which z refers to the axial direction and r to the radial direction. Because of symmetry of the material geometry and loading conditions, in Fig. 8 only one quarter of the longitudinal cross-section is considered up to $z=0.5 L_0$ (initial geometry). At the end face on this position the displacements in z direction are prescribed (constant velocity). In the simulations, near $z=0$, a geometric imperfection is introduced to initiate necking. This imperfection is cosine shaped, defined by

$$R_i = R_0 \left[1 - \frac{1}{2} (1 - \xi) \cos \left(\frac{\pi z}{\xi R_0} \right) \right] \quad 0 \leq z \leq \xi R_0 \quad (24)$$

with R_i the outer radius of the imperfection, R_0 the outer radius of the gauge section of the perfect bar, ξ the measure of the imperfection, $\xi = (2R_i(z=0) - R_0)/R_0$, and ζ controls the length of the imperfection. In the present calculations $\xi=0.9925$ and $\zeta=0.85$ which is equivalent to an area reduction of 1.5 percent at $z=0$. The nominal or engineering stress is defined by $F_z/(\pi R_0^2)$, where F_z is the applied tensile force.

The result of a numerical simulation at a nominal strain rate in the gauge section of $7.5 \cdot 10^{-3} [\text{s}^{-1}]$ is given in Fig. 9. The nominal stress and the elongation factor in the neck are depicted as a function of the nominal strain, together with the deformed meshes at different stages of the deformation. The nominal stress is defined as the tensile force divided by the original cross-sectional area and the draw ratio in the neck λ_N is calculated by division of the original cross-sectional area of the bar by the actual cross-sectional area in the middle of the specimen. During the simulation, the specimen initially deforms homogeneously, both in the elastic region and in the first part of the viscoplastic region ($a-b$). At some stage, the deformation localizes and a neck is formed ($b-d$), which propagates along the specimen as deformation continues ($d-e$). The neck propagation takes place under approximately steady-state conditions. The steady-state value of

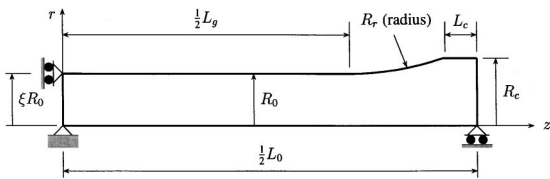


Fig. 8 Definition of the geometry of the longitudinal cross-section of the axisymmetrical tensile bar

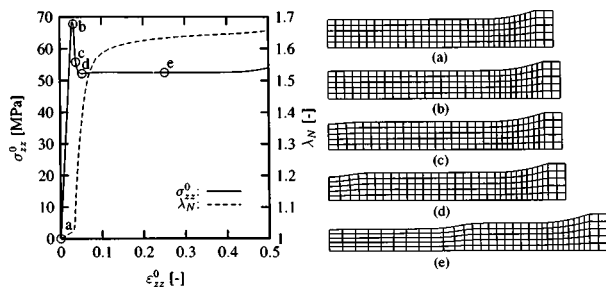


Fig. 9 Simulated tensile response of polycarbonate in terms of the nominal stress σ_{zz}^0 and the draw ratio in the neck λ_N versus the nominal strain ϵ_{zz}^0 at a nominal strain rate $\dot{\epsilon}_{zz}^0 = 7.5 \cdot 10^{-3} [\text{s}^{-1}]$. The deformed meshes at different stages of the simulation ($a-e$) are also shown.

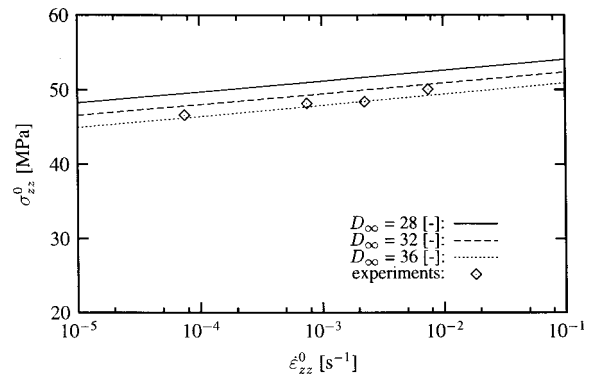


Fig. 10 Comparison of simulated and experimental values of the nominal stress during neck propagation at room temperature as a function of the nominal strain rate using different values of D_∞ . The lines are fitted through the results of the simulations.

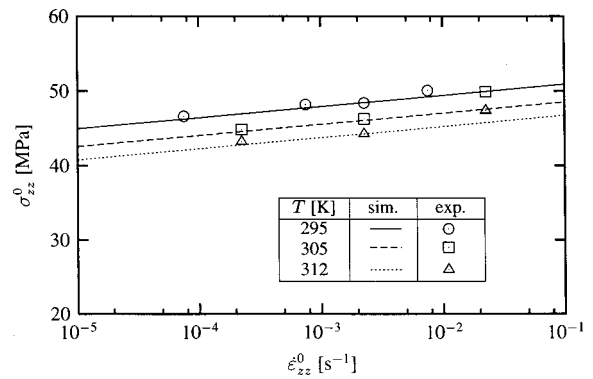


Fig. 11 Simulated and experimental values of the nominal stress during neck propagation versus nominal strain rate at different temperatures using $D_\infty = 36$. The lines are fitted through the results of the simulations.

the nominal stress during propagation of the neck proved to be independent of the geometry of the initial imperfection. The level of the draw ratio, on the other hand, was slightly influenced. The simulated levels of the nominal stress during neck propagation are compared to experimental data taken at room temperature in Fig. 10. Using the parameter set determined in the previous section, it proved impossible to predict the right stress level (see Fig. 10, $D_\infty = 28 [-]$). If it is assumed that the constitutive model is adequate, the quantification of the parameter set is indicated as the source of this discrepancy. Apparently, the friction between the compression platens and the sample also influenced the results of the compression test at low strain levels. To improve the description of the material behavior, the value of the softening parameter D_∞ was varied (see Fig. 10). A good description of the experimental data was obtained with a value of $D_\infty = 36 [-]$. To check this value, the simulations were repeated at temperatures of 305 and 312 [K] and compared to the experimental values of the nominal stress level during neck propagation at these temperatures. As can be observed in Fig. 11, the value $D_\infty = 36 [-]$ yields a reasonable description for all temperatures. This value was therefore adopted for the numerical simulations in the next sections.

5.2 The Mechanical Pretreatment: Mechanical Rejuvenation. The geometry of the axisymmetric polycarbonate samples that were preconditioned by one cycle of fixed-end torsion was shown in Fig. 4. The cylindrical surface of the bar is traction free,

and it is assumed that axial displacements are negligible. The twist $\varphi(t)$, dependent on the time t and defined per unit length of the bar, is applied at a low, constant, angular velocity $\dot{\varphi}$. Consequently, temperature effects have not been taken into account and the simulations were performed under isothermal conditions. The applied twist $\varphi(t)$ leads to a torque $M(t)$, and an axial force $F(t)$ resulting from the axially constrained ends.

To simulate the mechanical rejuvenation treatment a dedicated finite difference scheme was developed, assuming the relevant stress and strain quantities to be only a function of the radius and the loading time (homogeneous deformation over the length of the bar). The axisymmetric specimens were subjected to one full cycle of large strain torsion. First, the specimen was deformed up to a maximum twist (defined per unit length) of $\varphi = 0.25$ [rad mm⁻¹], which was applied at a constant angular velocity equal to $\dot{\varphi} = 9.1 \cdot 10^{-4}$ [rad s⁻¹ mm⁻¹]. After this, the direction of the twist was reversed, deforming the sample to a small negative twist value. Upon unloading of the sample, the cylindrical outer surface of the specimen approximately regains its initial state, which was verified during the experiments by monitoring a reference line on the sample.

Figure 12(a) shows the variation of the torque M as a function of the applied twist φ during the applied process history. Path ABC corresponds to the loading stage of the rejuvenation experiment and shows clearly the effect of intrinsic softening as the torque decreases after the yield point (B) has been reached. After a subsequent twist of about 0.1 [rad mm⁻¹] the torque level increases again as strain hardening sets in. The reversed twisting stage is represented by path CDE. The elastic unloading is shown by path EF. During this stage the cylindrical surface of the specimen regains its original geometry.

Figure 12(b) shows the distribution of the softening parameter D over the (dimensionless) radius r/R_a (R_a is the actual outer radius) at stages C and F in Fig. 12(a). It is clear that after the loading path ABC the softening parameter D in the outer layer of the specimen has almost reached its saturation level of $D_\infty = 36$. After the return twist, path CDEF, the softening parameter reaches its saturation level over $0.4 < r/R_a \leq 1$ indicating that the intrinsic softening effect has been removed over approximately 84 percent of the specimen volume.

The effect of this rejuvenation on a subsequent twist is shown in Fig. 12(a), path FGH, where it is clear that (a) the onset of yield begins at a considerably smaller torque than for the original material and (b) no intrinsic softening is observed.

The distribution of the stress components over the (dimensionless) radius at stage C and of the residual stress components at the end of the rejuvenation by fixed-end torsion at stage F are shown in Fig. 13. It is clear that at the end of the mechanical pretreatment the residual stress level of most components is negligible, whereas the component $\sigma_{\theta z}$ has a relatively high value in the core of the

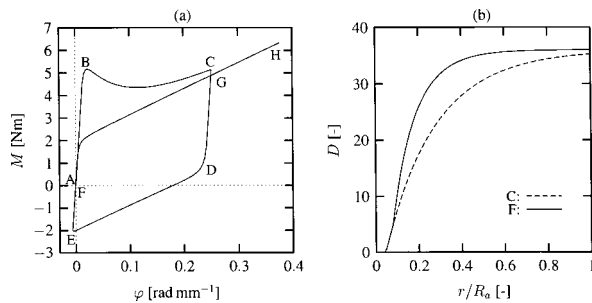


Fig. 12 Results of simulations of the mechanical preconditioning by torsion at an applied twist rate $\dot{\varphi} = 9.1 \cdot 10^{-4}$ [rad s⁻¹ mm⁻¹] at room temperature. (a) Torque versus twist per unit length and (b) distribution of the softening parameter D over the (dimensionless) radius at stages C and F in (a).

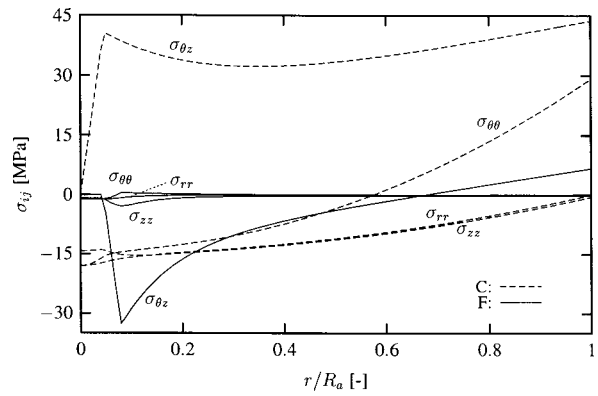


Fig. 13 Distribution of the relevant components of the Cauchy stress tensor over the (dimensionless) radius at stage C and the residual stress distribution after mechanical preconditioning at stage F in Fig. 12(a)

specimen. Although these residual stresses may effect the subsequent deformation behavior of the rejuvenated sample through the stress dependence of the viscosity (Eq. (14)), the elevated levels of $\sigma_{\theta z}$ only influence a small part of the specimen (approx. 10 percent of the volume). In order to minimize the influence of residual stresses in the experiments performed, the samples were allowed to relax unconstrained for a period of $10^3 - 10^4$ [s] before subsequent mechanical experiments were performed, thus allowing the residual stress levels to decrease.

Therefore, residual stresses will not be taken into account in simulations of tension and torsion tests on rejuvenated samples. Only the distribution of the softening parameter D over the radius after the rejuvenation, depicted by stage F in Fig. 12(b), will be used to characterize the “state” of the rejuvenated material.

5.3 Fixed-End Torsion of Rejuvenated Polycarbonate.

The fixed-end torsion simulations on rejuvenated samples were realized with a constant twist rate of $9 \cdot 10^{-4}$ [rad s⁻¹ mm⁻¹] at room temperature to a maximum twist of 0.4 [rad mm⁻¹]. The simulations were performed employing the same method as in the previous section, whereas the profile of the softening factor D , depicted in Fig. 12(b) at stage F, was taken as the initial situation. It should be noted that the residual stresses were not taken into account.

In Fig. 14(a) the variation of torque as a function of the twist φ is given for both the simulation and the experiment. Both compare well, which is a support for the values of $D_\infty = 36$ [-] and $H = 29$ [MPa] determined previously. The small deviations at lower twist levels, $\varphi < 0.05$ [rad mm⁻¹], are attributed to viscoelastic effects, which, as already stated before [30] are not adequately addressed in the single mode compressible Leonov model.

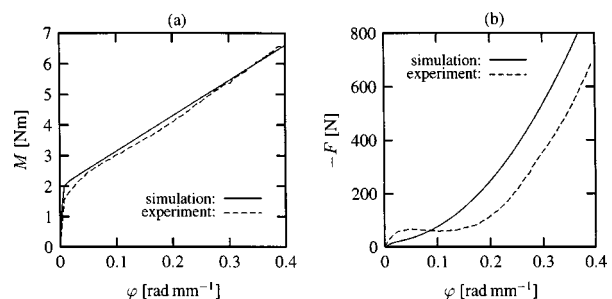


Fig. 14 Simulated and experimental curves of (a) torque versus twist per unit length and (b) compressive normal force versus twist per unit length for rejuvenated polycarbonate

Figure 14(b) shows a comparison of the experimental and numerical results of the normal force versus the twist φ , which is a more critical assessment of the constitutive model. It is clear that there are strong deviations between simulation and experiment. Again it should be emphasized that the viscoelastic behavior at low twist levels is not accurately described by the single mode compressible Leonov model. Also, at higher twist levels the model is not able to capture these secondary effects accurately, although the description improves and the deviations are, strangely enough, observed to be constant with a value of approximately 100 [N] for $0.2 < \varphi \leq 0.4$.

5.4 Uniaxial Extension of Rejuvenated Polycarbonate.

For the simulation of uniaxial extension of a rejuvenated sample of polycarbonate, again the finite element method is employed. In the finite element model, the distribution of the softening parameter D over the radius, depicted in Fig. 12(b) at stage F is specified as the initial condition. The distribution has been restricted to the gauge section of the specimen, since torsional deformations were only observed in this part. In the experiment and in the numerical simulation, the deformation rate imposed at the free end of the specimen corresponded with a nominal strain rate in the gauge section of $2.25 \cdot 10^{-3} [\text{s}^{-1}]$. To possibly trigger necking, exactly the same imperfection was used as in the tensile simulations of the untreated samples. For the present problem it was found that only meshes composed of ten elements or more in radial direction facilitated an accurate description of the initial distribution of D over the radius. Since during these experiments deformations were observed over the entire sample length, the mesh is equally distributed over the specimen.

Figure 15 shows the simulated and experimental true stress σ_{zz} versus $\lambda_{zz}^2 - \lambda_{zz}^{-1}$ for the mechanically rejuvenated polycarbonate tensile bar at a nominal strain rate of $2.25 \cdot 10^{-3} [\text{s}^{-1}]$. Small deviations between simulations and experiment can be observed,

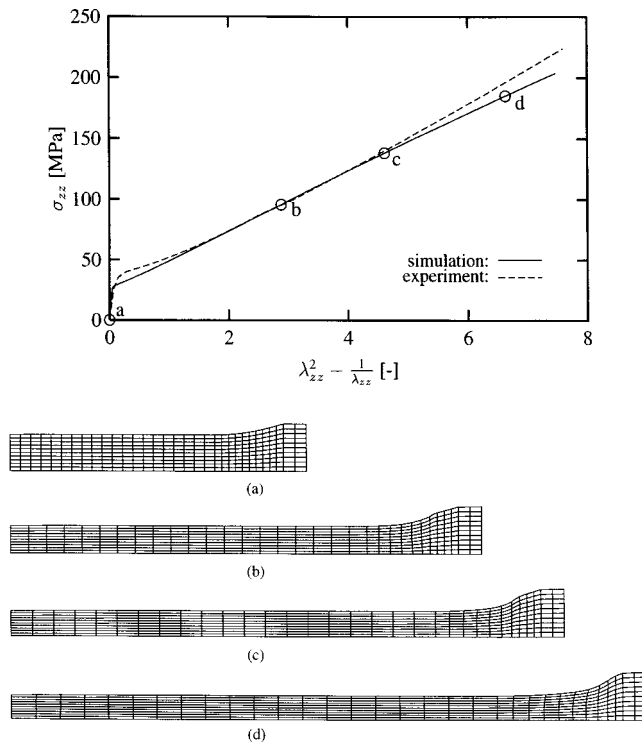


Fig. 15 Simulated and experimental true stress σ_{zz} versus $\lambda_{zz}^2 - \lambda_{zz}^{-1}$ during a tensile test at a strain rate of $2.25 \cdot 10^{-3} [\text{s}^{-1}]$ of a polycarbonate tensile bar, preconditioned in torsion. The indications (a–d) are related to the deformed meshes at different stages of the deformation.

which at small values of $\lambda_{zz}^2 - \lambda_{zz}^{-1}$ may be attributed to inaccuracies in the calculated value of D after rejuvenation by torsion. Other causes for the differences between simulated and experimental results may be viscoelastic effects, where the mechanical pretreatment might still influence the deformation behavior through a memory effect. As mentioned before, the single mode model used here will not capture these effects adequately.

Figure 15 also includes the deformed meshes at different stages of the deformation, which confirms the absence of necking, despite the presence of the imperfection. In contrast to the findings of Lu and Ravi-Chandar [32], this result strongly suggests that, in polycarbonate, strain softening is the main reason for localization phenomena.

6 Conclusion

In this study an extension of the compressible Leonov model has been presented, that captures the typical characteristics of the post-yield behavior of glassy polymers: intrinsic strain softening and strain hardening. Regarding the experimental assessment of the parameters needed for the model, it was found that the post-yield behavior during a compression test was too strongly influenced by barreling.

Mechanical rejuvenation by cyclic fixed-end torsion has been simulated, and the results have been used as initial conditions for numerical simulations of fixed-end torsion and uniaxial extension of rejuvenated polycarbonate. Comparison of these simulations with the experiments shows that although the post-yield behavior is described correctly by the compressible Leonov model, the deformation behavior at small strains is not captured. This is especially observed when comparing the axial forces during fixed-end torsion on rejuvenated samples. Although at higher strain levels there appeared to be a qualitative agreement, the behavior at low strain levels deviated strongly. It can therefore be concluded that the single mode compressible Leonov model is not valid with respect to second order effects during strain hardening.

On the other hand, the compressible Leonov model, extended with intrinsic strain softening and strain hardening, seems to be able to predict the transition from inhomogeneous (necking) to homogeneous deformation as a result of a mechanical pretreatment. It is therefore concluded that the intrinsic strain softening effect is the main cause for localization phenomena in polycarbonate.

References

- [1] G'Sell, C., Hiver, J. M., Dahouin, A., and Souahi, A., 1992, "Video Controlled Tensile Testing of Polymers and Metals Beyond the Necking Point," *J. Mater. Sci.*, **27**, p. 5031.
- [2] Boyce, M. C., Arruda, E. M., and Jayachandran, R., 1994, "The Large Strain Compression, Tension, and Simple Shear of Polycarbonate," *Polym. Eng. Sci.*, **34**, pp. 716–725.
- [3] Arruda, E. M., and Boyce, M. C., 1993, "Evolution of Plastic Anisotropy in Amorphous Polymers During Finite Straining," *Int. J. Plast.*, **9**, pp. 697–720.
- [4] Ward, I. M., 1983, *Mechanical Properties of Solid Polymers*, 2nd ed., Wiley, Chichester.
- [5] Haward, R. N., and Young, R. J., 1997, *The Physics of Glassy Polymers*, 2nd ed., Chapman & Hall, London.
- [6] Wu, P. D., and van der Giessen, E., 1993, "On Improved Network Models for Rubber Elasticity and Their Applications to Orientation Hardening in Glassy Polymers," *J. Mech. Phys. Solids*, **41**, pp. 427–456.
- [7] Haward, R. N., 1993, "Strain Hardening of Thermoplastics," *Macromolecules*, **26**, pp. 5860–5869.
- [8] Struik, L. C. E., 1978, *Physical Aging in Amorphous Polymers and Other Materials*, Elsevier, Amsterdam.
- [9] Struik, L. C. E., 1986, "Physical Aging: Influence on the Deformation Behavior of Glassy Polymers," *Failure of Plastics*, Brostow, W., and Corneliusen, R. D., eds., Hanser Publishers, Munich.
- [10] Hasan, O. A., and Boyce, M. C., 1993, "Energy Storage During Deformation in Glasses," *Polymer*, **34**, pp. 5085–5092.
- [11] G'Sell, C., 1986, "Plastic Deformation of Glassy Polymers: Constitutive Equations and Macromolecular Mechanisms," H. J. Queen et al., eds., *Strength of Metals and Alloys*, Pergamon Press, Oxford, pp. 1943–1982.
- [12] Aboulfaraj, M., G'Sell, C., Mangelincq, D., and McKenna, G. B., 1994,

- “Physical Aging of Epoxy Networks After Quenching and/or Plastic Cycling,” *J. Non-Cryst. Solids*, **172–174**, pp. 615–621.
- [13] Cross, A., and Haward, R. N., 1978, “Orientation Hardening of PVC,” *Polymer*, **19**, pp. 677–682.
- [14] Xie, L., Gidley, D. W., Hristov, A., and Yee, A. F., 1995, “Evolution of Nanometer Voids in Polycarbonate Under Mechanical Stress and Thermal Expansion Using Positron Spectroscopy,” *J. Polym. Sci.: Part B: Polym. Phys.*, **33**, pp. 77–84.
- [15] Hasan, O. A., Boyce, M. C., Li, X. S., Berko, S., 1993, “An Investigation of the Yield and Postyield Behavior and Corresponding Structure of Poly(Methyl Methacrylate),” *J. Polym. Sci., Part B: Polym. Phys.*, **31**, pp. 185–197.
- [16] Wu, P. D., and van der Giessen, E., 1995, “On Neck Propagation in Amorphous Glassy Polymers Under Plane Strain Tension,” *Int. J. Plast.*, **11**, pp. 211–235.
- [17] Bauwens, J. C., 1978, “A New Approach to Describe the Tensile Stress-Strain Curve of a Glassy Polymer,” *J. Mater. Sci.*, **13**, pp. 1443–1448.
- [18] Govaert, L. E., van Aert, C. A. C., Boekholt, J., 1997, “Temperature and Molecular Weight Dependence of the Strain Hardening Behavior of Polycarbonate,” *Proc. 10th Int. Conf. On Deformation, Yield and Fracture of Polymers*, The Institute of Materials, pp. 424–426.
- [19] Tervoort, T. A., Smit, R. J. M., Brekelmans, W. A. M., and Govaert, L. E., 1998, “A Constitutive Equation for the Elasto-Viscoplastic Deformation of Glassy Polymers,” *Mech. Time-Dep. Mat.*, **1**, pp. 269–291.
- [20] Hunter, S. C., 1983, *Mechanics of Continuous Media*, 2nd ed., Ellis Horwood Ltd., Chichester, U.K.
- [21] Boyce, M. C., Parks, D. M., and Argon, A. S., 1988, “Large Inelastic Deformation of Glassy Polymers. Part I: Rate Dependent Constitutive Model,” *Mech. Mater.*, **7**, pp. 15–33.
- [22] Bird, R., Armstrong, R., and Hassager, O., 1987, *Dynamics of Polymer Liquids*, Vol. 1: *Fluid Mechanics*, Wiley, New York.
- [23] Möglinger, B., and Fritz, U., 1991, “Thermal Properties of Strained Thermoplastic Polymers,” *Polym. Int.*, **26**, pp. 121–128.
- [24] Koenen, J. A., 1992, “Observation of the Heat Exchange During Deformation Using an Infrared Camera,” *Polymer*, **33**, pp. 4732–4736.
- [25] Boyce, M. C., Montagut, E. L., and Argon, A. S., 1992, “The Effects of Thermomechanical Coupling on the Cold Drawing Process of Glassy Polymers,” *Polym. Eng. Sci.*, **32**, pp. 1073–1085.
- [26] Van Krevelen, D. W., 1990, *Properties of Polymers: Their Correlation with Chemical Structure, Their Numerical Estimation and Prediction from Additive Group Contributions*, 3rd ed., Elsevier, Amsterdam.
- [27] Wu, W., and Turner, A. P. L., 1973, “Shear Bands in Polycarbonate,” *J. Polym. Sci., Polym. Phys. Ed.*, **11**, pp. 2199–2208.
- [28] Duckett, R. A., Goswami, B. C., Smith, L. S. A., Ward, I. M., and Zihlif, A. M., 1978, “The Yielding and Crazing Behavior of Polycarbonate in Torsion Under Superimposed Hydrostatic Pressure,” *Br. Polym. J.*, **10**, pp. 11–16.
- [29] Bauwens-Crowet, C., Bauwens, J. C., and Homès, G., 1969, “Tensile Yield Stress Behavior of Glassy Polymers,” *J. Polym. Sci.: Part A-2*, **7**, pp. 735–742.
- [30] Tervoort, T. A., Klompen, E. T. J., and Govaert, L. E., 1996, “A Multi-Mode Approach to Finite, Three-Dimensional, Nonlinear Viscoelastic Behavior of Polymer Glasses,” *J. Rheol.*, **40**, pp. 779–797.
- [31] Hasan, O. A., and Boyce, M. C., 1995, “A Constitutive Model for the Non-linear Viscoelastic Viscoplastic Behavior of Glassy Polymers,” *Polym. Eng. Sci.*, **35**, pp. 331–344.
- [32] Lu, J., and Ravi-Chandar, K., 1999, “Inelastic Deformation and Localization in polycarbonate Under Tension,” *Int. J. Solids Struct.*, **36**, pp. 391–425.